ACS OMEGA

http://pubs.acs.org/journal/acsodf

Article

Electrochemical Sensors Based on a Composite of Electrochemically Reduced Graphene Oxide and PEDOT:PSS for Hydrazine Detection

Hemas Arif Rahman, Mohamad Rafi, Budi Riza Putra, and Wulan Tri Wahyuni*

Cite This: *ACS Omega* 2023, 8, 3258−3269

Read Online

ACCESS | Metrics & More | Article Recommendations

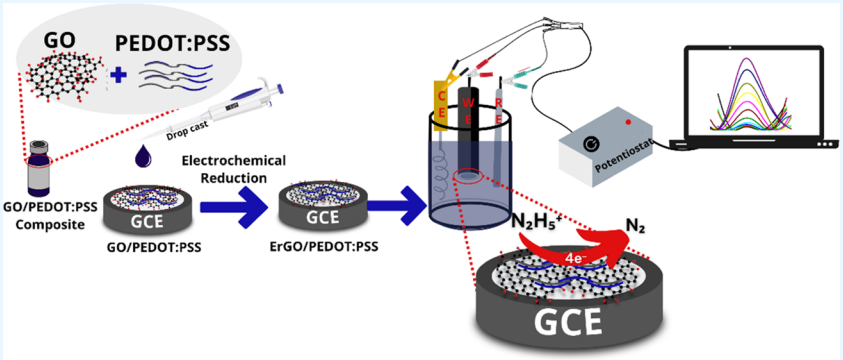

ABSTRACT: In this study, hydrazine sensors were developed from a composite of electrochemically reduced graphene oxide (ErGO) and poly(3,4-ethylenedioxythiophene):poly(styrenesulfonate) (PEDOT:PSS), deposited onto a glassy carbon electrode (GCE). The structural properties, electrochemical characterization, and surface morphologies of this hydrazine sensor were characterized by Raman spectroscopy, Fourier transform infrared (FTIR) spectroscopy, electrochemical impedance spectroscopy (EIS), and scanning electron microscopy (SEM). In addition, the proposed hydrazine sensor also demonstrates good electrochemical and analytical performance when investigated using cyclic voltammetry (CV), differential pulse voltammetry (DPV), and amperometry techniques under optimal parameters. Using these investigated parameters, DPV and amperometry were chosen as techniques for hydrazine measurements and showed a linear range of concentration in the range of 0.2−100 μM. The obtained limits of detection and limits of quantitation for hydrazine measurements were 0.01 and 0.03 μM, respectively. In addition, the proposed sensor demonstrated good reproducibility and stability in hydrazine measurements in eight consecutive days. This fabricated hydrazine sensor also exhibited good selectivity against interference from Mg^{2+}, K^+, Zn^{2+}, Fe^{2+}, Na^+, NO_2^-, CH_3COO^-, SO_4^{2-}, Cl^-, ascorbic acid, chlorophenol, and triclosan and combined interferences, as well as it depicted %RSD values of less than 5%. In conclusion, this proposed sensor based on GCE modified with ErGO/PEDOT:PSS displays exceptional electrochemical performance for use in hydrazine measurements and have the potential to be employed in practical applications.

1. INTRODUCTION

IPB Hydrazine is a hazardous chemical, used extensively in industrial applications, such as explosives,[1] corrosion inhibitors,[2] pesticides and herbicides,[3] rocket and aircraft propellants,[4] fuel cells,[5] catalysis,[6] emulsifiers,[7] and pharmaceutical compounds.[8] Furthermore, hydrazine and its derivatives are considered neurotoxin,[9] carcinogenic,[10] mutagenic,[11] and teratogenic[12] substances that can be absorbed by the human body, resulting in severe harm to the skin,[13] kidneys,[14] and liver.[15] In addition, long-term exposure to hydrazine could affect the central nervous system in the body, leading to genetic diseases.[16] Therefore, the United States Environmental Protection Agency (EPA) regulations indicate that the total concentration of hydrazine in drinking water with the threshold limit value (TLV) should be no more than 10 ppb.[17] As a result, developing a sensitive, rapid, and reliable technique for determination is highly important for quality assessment of water.

Several analytical methods have been reported for the determination of hydrazine concentration, based on titrimetry,[18] gas chromatography-mass spectrometry,[19] high-performance liquid chromatography-tandem mass spectrometry,[20] fluorescence,[21] chemiluminescence,[22] and surface-enhanced Raman spectroscopy.[23] However, these methods employ

Received: October 21, 2022
Accepted: December 28, 2022
Published: January 9, 2023

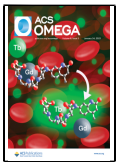

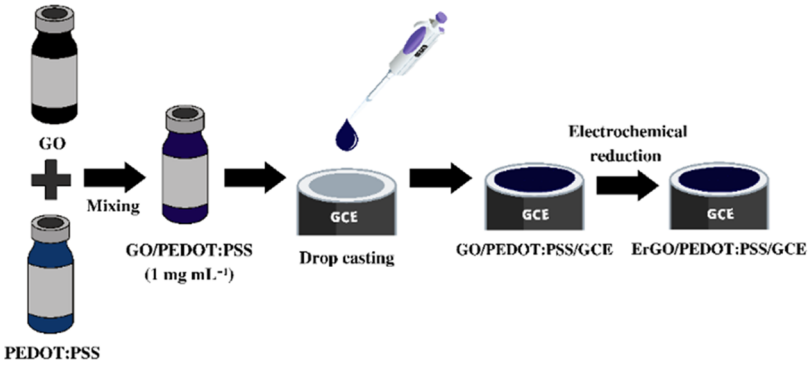

Figure 1. Schematic Illustration of the Modification of glassy carbon electrode (GCE) with the ErGO/PEDOT:PSS composite.

various reagents, require specific skills to operate sophisticated instruments, and are time consuming and thus not practical for in situ analysis. Alternatively, electrochemical methods offer an attractive approach for hydrazine measurements due to their low cost, simple preparation, rapid response, high sensitivity, and potential as portable devices.[24−29] For these reasons, we selected electrochemical methods for hydrazine measurements for this present study. There are a plethora of electroanalytical methods that have been developed to provide electrochemical sensing of hydrazine based on the platform of the modified carbon electrode.[30−40] In addition, we have reported the utilization of the composite material of electrochemically reduced graphene oxide (ErGO) and conductive polymer-modified electrode for uric acid detection,[41] but it remains interesting to explore our developed sensing platform for the detection of novel electroactive substance hydrazine. We expect that our developed sensing platform could be a versatile electrode for the detection of different electroactive substances.

As a two-dimensional nanomaterial, electrochemically reduced graphene oxide (ErGO) has been intensively investigated in the fields of electroanalysis,[42−45] energy storage devices,[46−48] and electrocatalysis,[49−51] due to its excellent catalytic activity[52] and chemical stability.[53] In addition, poly(3,4-ethylenedioxythiophene):poly(styrenesulfonate) or PEDOT:PSS (previously used in uric acid sensors) is beneficial for enhancing the electrocatalytic activity and conductivity of the graphene oxide (GO) materials.[54−56] Therefore, in this study, we highlight the employment of the composite materials of ErGO with PEDOT:PSS deposited onto a glassy carbon electrode (GCE) for use as a hydrazine sensor. To the best of our knowledge, no previous work has described the combination of ErGO and PEDOT:PSS for development as a sensing platform for hydrazine detection. It is expected that the as-prepared electrode (GCE modifying a composite of ErGO and PEDOT:PSS) could exhibit excellent analytical performances for use as a hydrazine sensor, either in the synthetic solution or in real samples compared to that using a bare GCE.

2. EXPERIMENTAL METHODS

2.1. Materials. Graphite powder, poly(3,4-ethylenedioxythiophene):poly(styrene-4-sulfonate) (PEDOT:PSS) (CAS: 155090-83-8), $N_2H_4{\cdot}2HCl$ (CAS: 5341-61-7), concn H_2SO_4, $KMnO_4$, H_2O_2 30%, Na_2HPO_4, NaH_2PO_4, KCl, *para*-dimethylamino benzaldehyde (PDAB) (CAS: 100-10-7), $Zn(CH_3CO_2)_2{\cdot}2H_2O$, $NaNO_3$, KCl, $FeSO_4$, $Mg(CH_3CO_2){\cdot}4H_2O$, and concn HCl were obtained from Sigma-Aldrich Ltd and used without further purification. Deionized water was used throughout all experiments. Scanning electron microscopy−energy dispersive X-ray spectroscopy (SEM−EDS) images were obtained using an FEI Quanta 650 scanning electron microscope equipped with an Energy Dispersive Spectrometer OXFORD.

2.2. Instrumentation. A PalmSens Emstat 3 (ES316U669) device running with PS Trace 5.9 software was used for the electrochemical studies. Meanwhile, a PalmSens 4.0 Potentiostat/Galvanostat/Impedance Analyzer (Palms Sens Compact Electrochemical Interfaces, The Netherlands) was employed to perform electrochemical impedance spectroscopy (EIS) studies. Raman spectra were obtained using HORIBA HR an Evolution Raman Microscope with laser excitation at 514 nm. An infrared spectrum was obtained using a Bruker Fourier transform infrared (FTIR) Tensor 37. The images of the surface-modified electrode was recorded by scanning electron microscope−energy dispersive X-ray spectroscopy (SEM−EDS) (FEI Quanta 650, Oxford, U.K.).

2.3. Synthesis of Graphene Oxide. Graphene oxide (GO) was synthesized using modified Hummer's method.[41] Here, 1 g of graphite and 0.5 g of $NaNO_3$ were added to 25 mL of concn H_2SO_4 and stirred at 0 °C for 1 h. Next, 3 g of $KMnO_4$ was slowly added and the temperature was maintained below 20 °C. The solution was then continuously stirred for 1 h and left for 30 min at room temperature. Subsequently, 50 mL of deionized water was added to the mixture to produce a heat excess to 90−95 °C (an exothermic reaction). The mixture was then stirred for 1 h and left for 15 min thereafter. Finally, about 50 mL of 30% H_2O_2 was added to the mixture to terminate the reaction. The resulting mixture was then stirred for 1 h and cooled thereafter at room temperature. The resulting GO solution was washed with deionized water to remove the metal ions, then filtered and dried in an oven. The obtained GO powder was then characterized using Raman spectroscopy.

2.4. Preparation of ErGO/PEDOT:PSS Composite-Modified GCE. The preparation of a composite solution of GO/PEDOT:PSS was performed following this procedure. First, the solution of GO was dispersed in a PEDOT:PSS solution (1 mg mL^{-1} in deionized water) at a ratio of 1:1. The GO/PEDOT:PSS composite was then sonicated for 1 h, followed by a drop of about 4 μL cast onto the surface of the GCE. The modified GCE was then dried in an oven at 100 °C for 5 min. The obtained GO/PEDOT:PSS film on the surface of the GCE was then reduced to ErGO-modified PEDOT:PSS (ErGO/PEDOT:PSS). To perform these reduction processes, a cyclic voltammetry technique was applied with a potential window between 0 and −1.3 V at a scan rate of 50 mV s^{-1} for

https://doi.org/10.1021/acsomega.2c06791
ACS Omega 2023, 8, 3258−3269

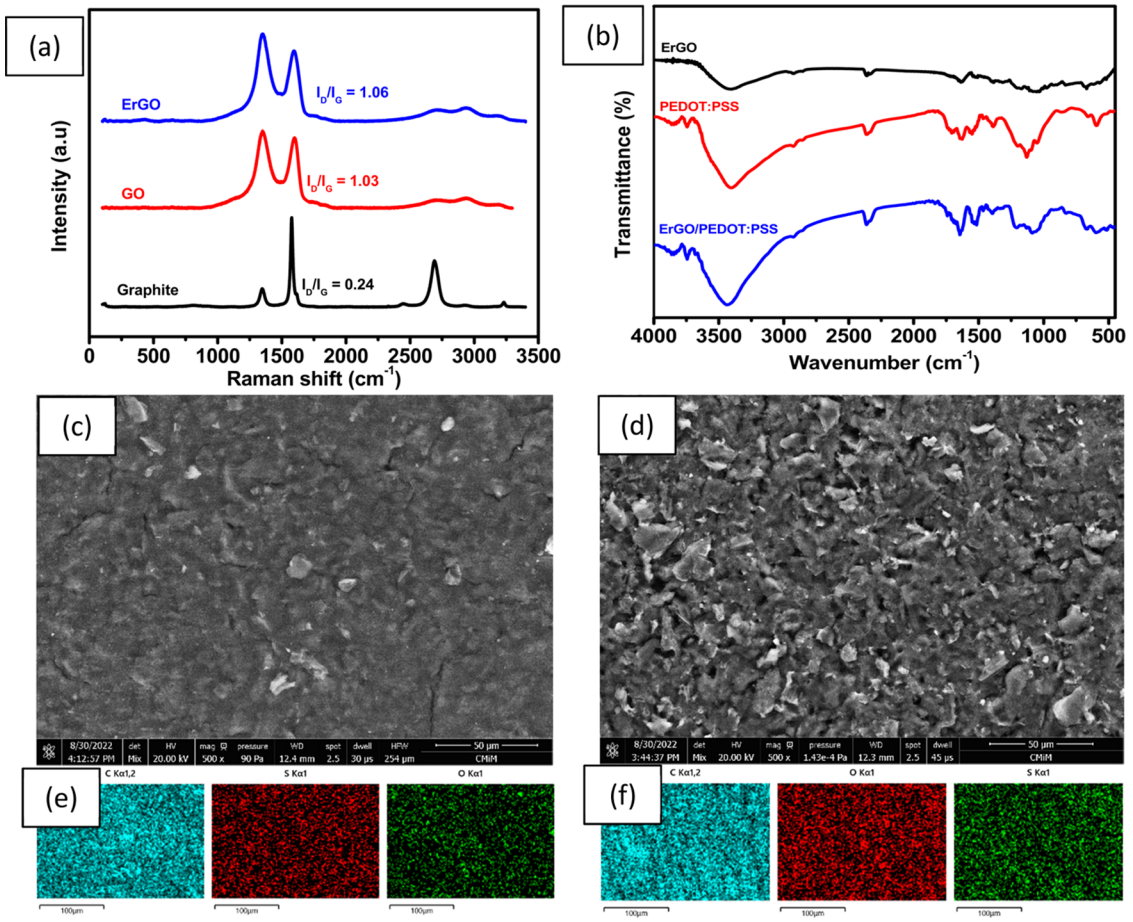

Figure 2. (a) Raman spectrum of graphite, graphene oxide, and electrochemically reduced graphene oxide (ErGO); (b) FTIR spectrum of ErGO, PEDOT:PSS, and ErGO/PEDOT:PSS composites, (c) SEM image of ErGO, (d) SEM image of ErGO/PEDOT:PSS, (e) elemental mapping of C, O, and S in ErGO, and (f) elemental mapping of C, O, and S in ErGO/PEDOT:PSS.

20 cycles in an electrolyte solution of 0.1 M KCl. The obtained electrodes (ErGO/PEDOT:PSS-modified GCE) were then cleaned with deionized water and dried at room temperature. Figure 1 displays the schematic illustration of the preparation of the ErGO/PEDOT:PSS composite and modification of GCE with ErGO/PEDOT:PSS. The ErGO/PEDOT:PSS was then characterized using FTIR and SEM−EDS.

2.5. Linearity, Limit of Detection (LOD), and Limit of Quantitation (LOQ). Linearity was evaluated by measuring the hydrazine solution in a concentration range of 0.2−100 μM (n = 3) in 0.1 M phosphate buffer at pH 7 using ErGO/PEDOT:PSS/GCE. The concentrations were measured using differential pulse voltammetry (DPV) and amperometry. DPV was performed in the potential window from −0.3 to +0.85 V with a scan rate of 50 mV s^{-1} in triplicates. Amperometry was performed at a potential of 0.3 V with $t_{interval}$ of 0.1 s and $t_{running}$ of 20 s. From the measurement of hydrazine in the concentration range of 0.2−100 μM in triplicate, it was found that there was a calibration curve with a coefficient of determination (R^2). DPV and amperometry techniques were selected for further investigation of hydrazine measurements, as they provide the highest sensitivity, as indicated by $R^2 \approx 1$. Linearity was evaluated from the relationship between the concentration of the solution and the current response of hydrazine measurements. The limit of detection (LOD) was investigated based on 3σ, where σ is the standard deviation of response derived from the linear equation of hydrazine measurements in triplicate. The limit of quantification (LOQ) was estimated from the LOD value, multiplied by three.

2.6. Reproducibility, Stability, and Selectivity. The reproducibility was evaluated by preparing four different electrodes of ErGO/PEDOT:PSS-modified GCE. The electrodes were then employed using measurements of 60 μM hydrazine solution in 0.1 M pH 7 phosphate buffer. The evaluation of electrode stability was also performed by measuring 60 μM hydrazine solution in 0.1 M phosphate buffer at pH 7, using the same electrode for 8 consecutive days. The study of sensor selectivity was performed by measuring 60 μM hydrazine solution in the presence of zinc acetate, magnesium acetate, iron acetate, sodium nitrite, potassium chloride, and combined interferences as interfering agents, prepared from a 1 × 10^{-3} M standard solution and dissolved in 0.1 M phosphate buffer at pH 7. Preparation for the combined interference was measured by adding all 60 μM interferences to a 10 mL volumetric flask containing 60 μM hydrazine, then diluting using 0.1 M phosphate buffer at pH 7. Before and after the addition of interfering agents, the hydrazine solution was measured three times using the differential pulse voltammetry technique. All electrochemical measurements were conducted using the differential pulse voltammetry technique at a potential window from −0.30 to +0.85 V, at a scan rate of 50 mV s^{-1}, a potential step of 10 mV, a potential pulse of 50 mV, and a pulse time of 50 ms.

https://doi.org/10.1021/acsomega.2c06791
ACS Omega 2023, 8, 3258−3269

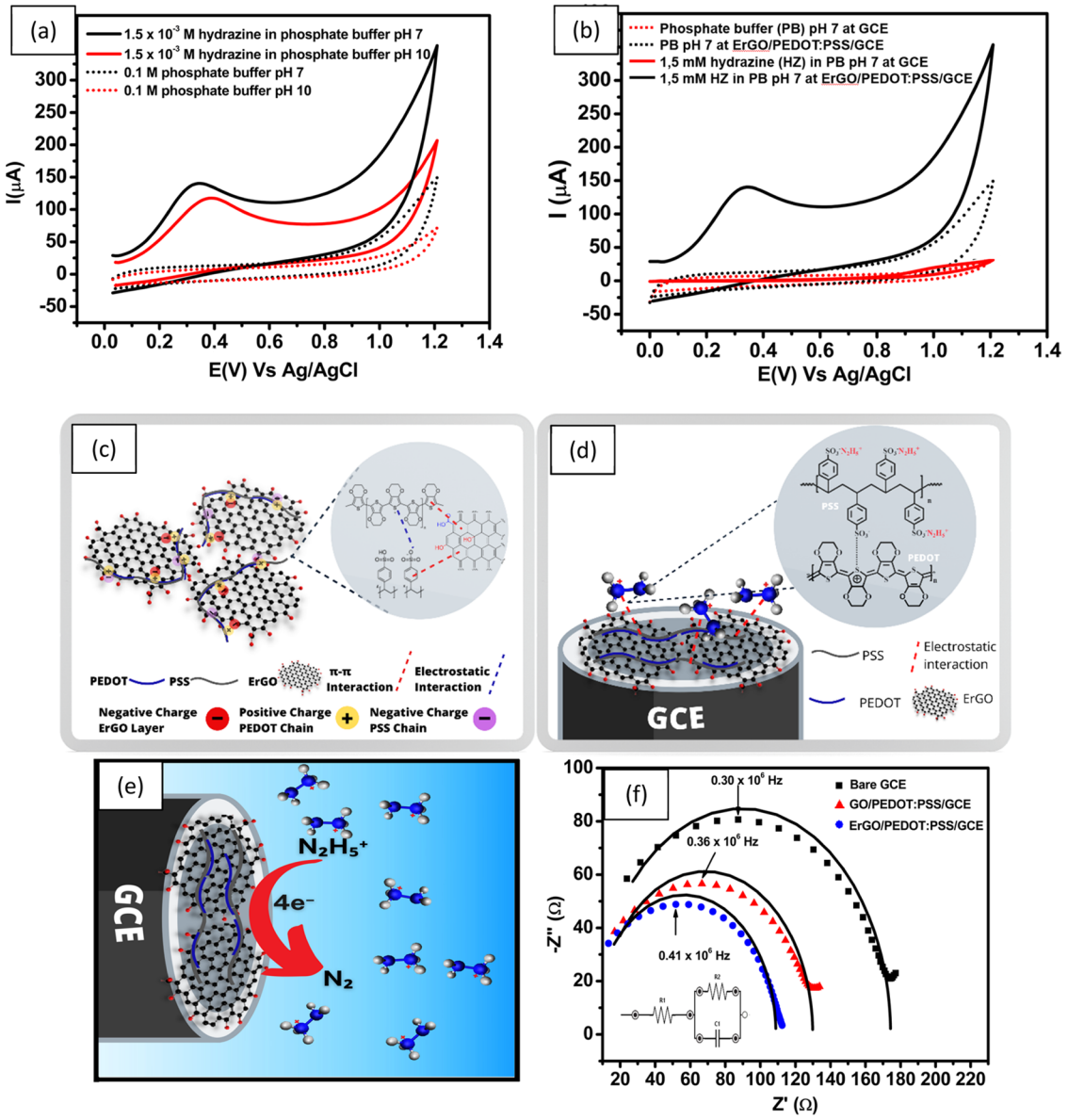

Figure 3. (a) Cyclic voltammogram measuring 1.5 × 10^{-3} M hydrazine with phosphate buffer at pH 7 and pH 10 obtained with ErGO/PEDOT:PSS/GCE; (b) cyclic voltammogram at a scan rate of 100 mV s^{-1} of 0.1 M pH 7 phosphate buffer and 1.5 × 10^{-3} M hydrazine in 0.1 M phosphate buffer at pH 7, measured using bare GCE and ErGO/PEDOT:PSS/GCE; (c) schematic illustration of the interaction between electrochemically reduced graphene oxide (ErGO) with PEDOT:PSS and (d) of the interaction between the hydrazinium cation with the ErGO/PEDOT:PSS composite on the surface of glassy carbon electrode (GCE); (e) mechanism of hydrazine oxidation at the surface of ErGO/PEDOT:PSS/GCE, (f) Nyquist plot obtained for three different electrodes (bare GCE, GO/PEDOT/GCE, and ErGO/PEDOT:PSS/GCE) for measuring 1 mM $K_3[Fe(CN)_6]$ in 0.1 M KCl solution at a frequency range from 1 × 10^6 to 5 × 10^3 Hz, E_{dc} = 0 V, E_{ac} = 10 mV at an open circuit potential.

2.7. Measurement of Hydrazine from River Water. The modified electrode was then employed to measure hydrazine in the sample obtained from river water using standard addition techniques and investigated by the electrochemical techniques. Initially, the sample of river water was diluted by an equal volume, and then by 1 × 10^{-3} M hydrazine solution in 0.1 M pH 7 phosphate buffer added stepwise in a concentration series of 20−100 μM. The sample solution and the spiked hydrazine were then analyzed using the DPV technique in the potential range from −0.3 to +0.85 V at a scan rate of 50 mV s^{-1}, a potential step of 10 mV, a potential pulse of 50 mV, and a pulse time of 50 ms. The concentration of hydrazine in the river water sample was then calculated using multiple point linear regression by defining the value of the x-intercept. The concentration of hydrazine in the river water sample determined by the electrochemical technique was then compared with the standard methods using spectrophotometric techniques (NSA 1996). The principle of hydrazine detection using the spectrophotometric method was based on the reaction of *para*-dimethylamino benzaldehyde (PDAB) with hydrazine under acidic conditions to form a yellow compound. Briefly, hydrazine solution was prepared in the concentration range of 0.23−3.81 μM and then transferred to an Erlenmeyer flask. Then, 5 mL of PDAB at a concentration of 1.82% and 2.5 mL of concn HCl were added to the Erlenmeyer flask and allowed to stand for 10 min. The

https://doi.org/10.1021/acsomega.2c06791
ACS Omega 2023, 8, 3258−3269

absorbance of the solution was then measured using a UV−vis spectrophotometer at a maximum wavelength of 458 nm. The hydrazine content in the sample of river water was then calculated from the calibration curve, and its results were compared with electrochemical techniques using statistical analysis, namely Student's *t*-test with a 95% confidence interval.

3. RESULTS AND DISCUSSION

A composite film of GO/PEDOT can be reduced into ErGO/PEDOT:PSS on the surface of GCE by applying potential scanning for up to 40 cycles.[41] The potential scanning of the GO/PEDOT:PSS composite can partially remove the oxygen functional groups in the GO chemical structures, but it does not destroy the backbone structure of PEDOT:PSS.[57] In addition, this electrochemical method provides a safer approach for reducing GO materials and maintaining the electroactivity of PEDOT:PSS relative to conventional GO reduction. The voltammogram of the reduction process of GO/PEDOT:PSS with potential cycling at 50 mV s^{-1} in 0.1 M KCl from 0 to −1.3 V vs Ag/AgCl (data not shown) provides cathodic current at a potential of −0.4 V that indicated a reduction of hydroxyl functional groups in the chemical structure of GO.[58] The cathodic current increased linearly for up to 20 cycles due to the enhancement of the reduction process of GO materials.

3.1. Surface Characterization of the Modified Electrode by Raman, FTIR, and SEM Techniques. Raman spectroscopy is used extensively to examine graphite and its derivatives. It is excellent for studying disorders and flaws in crystal structures. Figure 2a displays the Raman spectra of graphite, graphene oxide, and ErGO. For graphite, GO, and ErGO, the D band is visible at 1346, 1350, and 1351 cm^{-1}, respectively, and the G bands appear at 1577, 1604, and 1603 cm^{-1}. All sp^2 carbon forms share the G band, which results from the stretching of the C−C bond.[58] This band is created by first-order Raman scattering. The D band is associated with vacancies, dislocations, and cracks in the graphene layer and indicates the presence of defects in the graphite material.[49] In addition, ErGO also has 2D bands which have higher intensity than GO. This is because after the reduction of GO to ErGO, the remaining number of functional group residues containing oxygen decreases, causing ErGO to accumulate. The I_D/I_G ratio for GO was 1.03. Due to the restoration of sp^2 carbon and increased dislocations in the graphene layer as a result of missing oxygen groups, and the I_D/I_G for ErGO increased (1.06) after reduction.[50]

Figure 2b displays the FTIR spectra of ErGO, PEDOT:PSS, and ErGO/PEDOT:PSS. Vibration peaks for ErGO film appear at 1050 cm^{-1} (C−O stretching), 1580 cm^{-1} (C═C stretching), 1750 cm^{-1} (C═O stretching), and at 3500 cm^{-1} (O−H stretching), which shows a large peak. FTIR spectra were used to analyze the vibration of functional groups in PEDOT:PSS and ErGO/PEDOT:PSS films. The vibrational peaks in both IR spectra correspond to the thiophene backbone in the PEDOT:PSS structure at 1650 cm^{-1} (C═C stretching), 1510 cm^{-1} (C═C aromatic stretching), and 1300 cm^{-1} (C−C stretching). Additionally, peaks at 990 cm^{-1} and 850 cm^{-1} are related to S−O bands in the PSS structure as well as the C−S stretching peak at 1200 cm^{-1} in the EDOT structure.[41]

To characterize the surface morphology of the modified electrode, SEM analysis with elemental mapping (EDX spectrum) was applied to ErGO and ErGO/PEDOT:PSS materials. As shown in Figure 2c, the surface of ErGO has a wrinkled and flake-like morphology with an orientation similar to a randomly crumpled sheet. This wrinkled structure might be due to the restacking of rGO layers as a result of the electrochemical reduction process toward GO materials, which provides a gap between the nanosheets.[59] The gap between these nanosheets can range from several nanometers to micrometers and is expected to be much thicker than single-layer graphene. In addition, this is evident from the EDX spectrum of ErGO, which contains around 85.8% C, 13.4% O, and 0.7% S, which suggests that ErGO was formed evenly, as shown in Figure 2e. The presence of a low concentration of sulfur in ErGO may come from H_2SO_4 during GO synthesis, which is intercalated into the graphite-based material.[60] When PEDOT:PSS was incorporated into ErGO (Figure 2d), the gap between nanosheets becomes filled with PEDOT:PSS, suggesting that both $\pi-\pi$ and electrostatic interactions occur between ErGO and PEDOT:PSS.[61] Elemental analysis of ErGO/PEDOT:PSS from the EDX spectrum in Figure 2f reveals contents of carbon, oxygen, and sulfur of 77.6, 21, and 1.3%, respectively. Based on this, the increasing concentration of sulfur might be due to the formation of ErGO/PEDOT:PSS, which suggests that PEDOT:PSS now occupies the interlayer of nanosheets.[62] The variation in the content of other elements in the ErGO/PEDOT:PSS composite could be correlated with local concentrations of components when EDX analysis is performed.

3.2. Electrochemical Behavior of GCE Modified with ErGO/PEDOT:PSS. The electrochemical behavior of 1.5 × 10^{-3} M hydrazine is shown using pH 7 and pH 10 phosphate buffer in Figure 3a. Based on Figure 3a, there is a shift in the peak oxidation potential of hydrazine at pH 7 with ErGO/PEDOT:PSS/GCE electrodes to a potential of 0.34 V vs Ag/AgCl compared to pH 10, recorded at 0.39 V vs AgCl. In addition, the peak current for hydrazine oxidation at pH 7 is 76 μA, while at pH 10, it is 74 μA. This means that at pH 7, it is easier to oxidize using hydrazine than at pH 10 using ErGO/PEDOT:PSS/GCE, based on the recorded potential value. Therefore, pH 7 phosphate buffer was used in the following test.

To gain insight into the electrochemical behavior of the modified electrode, cyclic voltammogram of 0.1 M pH 7 phosphate buffer as an electrolyte and 1.5 × 10^{-3} M hydrazine in the electrolyte were recorded at a scan rate of 100 mV s^{-1}. The voltammograms were compared with those obtained with the bare GCE and ErGO/PEDOT:PSS-modified GCE under similar experimental conditions. As shown in Figure 3b, 0.1 M pH 7 phosphate buffer provides a very small signal when measured with bare GCE. However, when ErGO/PEDOT:PSS-modified GCE was used to measure 1.5 × 10^{-3} M hydrazine in a pH 7 electrolyte, a higher background current was observed than in bare GCE. This result was expected, as the modification of the GCE surface with ErGO/PEDOT:PSS was expected to alter the morphology of the surface of the electrode due to an increase of the surface roughness and a number of electroactive sites. In addition, this increase in electroactive sites and improved surface roughness will lead to enhanced conductivity and electrocatalytic activity of the ErGO/PEDOT:PSS composite, resulting in a higher background current. Furthermore, when ErGO/PEDOT:PSS-modified GCE was employed for the measurement of 1.5 × 10^{-3} M hydrazine, the oxidation peak was shifted to a potential

https://doi.org/10.1021/acsomega.2c06791
ACS Omega 2023, 8, 3258−3269

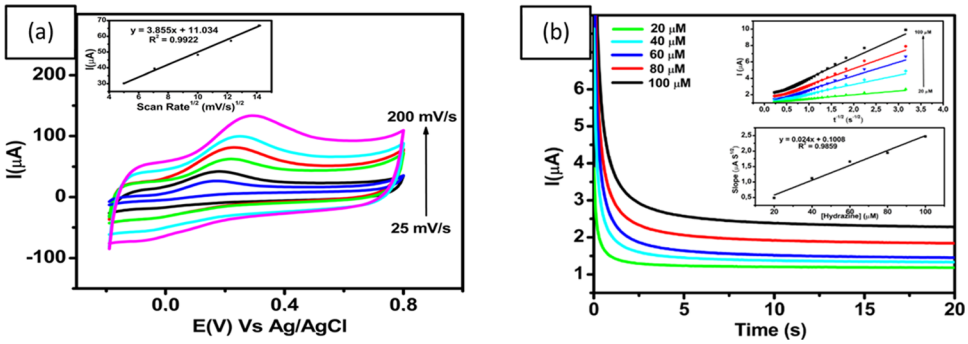

Figure 4. (a) Voltammogram of 100 μM hydrazine in 0.1 M phosphate buffer at pH 7 with different scan rates of ErGO/PEDOT:PSS/GCE. Inset: linear correlation between the square root of scan rate with the peak current of hydrazine oxidation, (b) amperometric curves obtained from different concentrations of hydrazine (20−100 μM) in 0.1 M pH 7 phosphate buffer at a scan rate of 50 mV s^{-1} and an applied potential (E_{dc}) of 0.3 V vs Ag/AgCl. Inset: the calibration plot of hydrazine concentration versus the current peak of hydrazine oxidation.

of 0.33 V vs Ag/AgCl, where bare GCE, 1.01 V vs Ag/AgCl was observed. In addition, the intensity of the peak current (I_{pa}) for hydrazine oxidation measured with ErGO/PEDOT:PSS-modified GCE was 30 times higher than that detected with bare GCE. This increase in the value of I_{pa} and hydrazine oxidation at lower applied potential could be assigned to synergistic effects between the larger surface area of ErGO/PEDOT:PSS composites with better electron transfer to the surface of modified electrodes. The enhanced electrocatalytic activity of the ErGO/PEDOT:PSS composite was also due to the nature of hydrazine as an electron donor, thus facilitating the charge transfer processes on the surface of the modified electrode. From the above results, it can be concluded that the ErGO/PEDOT:PSS composite is suitable for electrocatalytic and sensing applications, especially for hydrazine detection.

It is already known that the presence of hydrazine species in aqueous media can be differentiated as a function of pH.[17] The predominant species of hydrazine at acidic to neutral pH is the hydrazinium cation ($N_2H_5^+$), while N_2H_4 is the main species when the pH of the solution is higher than 9.7.[63] In this work, the pH of the hydrazine solution was adjusted using pH 7 phosphate buffer, so it can be expected that $N_2H_5^+$ will be the predominant species. The positive charge of this species ($N_2H_5^+$) is expected to undergo an electrostatic attraction with a negative charge in polymeric chains of PEDOT:PSS and ErGO that facilitate the oxidation reaction toward the hydrazine molecules.

Figure 3c shows the schematic illustration of chemical bonding between electrochemically reduced graphene oxide (ErGO) with the conductive polymer (PEDOT:PSS). This interaction is due to $\pi-\pi$ interactions, which co-exist in graphene layers and PEDOT:PSS. This type of interaction causes PEDOT:PSS to be adsorbed to the surface of graphene and its single extended polymer chains with linear conformations, which can be intercalated between GO layers.[64] In addition, GO layers possess many oxygen-containing groups including epoxy, carbonyl, and hydroxyl groups, carrying negative charges. These negative charges of GO layers may bond with positively charged PEDOT chains and negatively charged PSS chains through electrostatic interactions. However, when ErGO/PEDOT:PSS composite materials were employed for hydrazine detection, an electrostatic attraction arose between sulfonic functional groups ($-SO_3^-$) from the chain structure of PSS with the hydrazinium cations ($N_2H_5^+$) to form the ($-SO_3^-$ $N_2H_5^+$) complex,[65] as shown in Figure 3d. This complex causes the electrochemical reaction of hydrazine on the surface of GCE modified with ErGO/PEDOT:PSS due to the current flow between the working and counter electrodes, which is proportional to the hydrazine concentration.

In addition, at pH 7, as shown in Figure 3e, the electrochemical oxidation of hydrazine species ($N_2H_5^+$) produces nitrogen gas and hydronium ions involving a 4-electron process with a second step as the rate-determining step (rds) (see the mechanism below). The first reaction is the dissociation of the hydrazinium cation into hydrazine, and the third reaction produces nitrogen gas as a rapid step of hydrazine oxidation.

$$N_2H_5^+ (aq) \rightleftharpoons N_2H_4 (aq) + H^+ (aq) \quad (1)$$

$$N_2H_4 (aq) \xrightarrow{rds} N_2H_4^{\bullet +} (aq) + e^- \quad (2)$$

$$N_2H_4^{\bullet +} (aq) \xrightarrow{fast} N_2 (g) + 4H^+ (aq) + 3e^- \quad (3)$$

3.3. Electrochemical Impedance Spectroscopy Studies of the Modified Electrode. EIS studies were performed on three different electrodes (bare GCE, GO/PEDOT:PSS-modified GCE, and ErGO/PEDOT:PSS) to study electron transfer resistance at the electrode/electrolyte interface. These three electrodes were investigated by measuring 1 mM $K_3[Fe(CN)_6]$ in 0.1 M KCl solution with a frequency range from -1×10^6 to 5×10^3 Hz, E_{ac}= 10 mV at an open constant potential. As shown in Figure 3e, all Nyquist plots were obtained from each modified electrode that had different diameters of the semicircle in the high-frequency region. The diameter of a semicircle is attributed to the charge transfer process at the electrode/electrolyte interface and is equivalent to the charge transfer resistance (R_2). The value of R_2 can be calculated by fitting the obtained Nyquist plot with the equivalent Randles circuit, as shown in the inset of Figure 3f.

From the calculations using the equivalent circuit, the R_2 obtained in series has been steadily decreasing from bare GCE (169.6 Ω) to GO/PEDOT:PSS/GCE (122.5 Ω). The lower value of resistance obtained from GO/PEDOT:PSS/GCE indicated that the GO/PEDOT:PSS composite promotes electron transfer and thus enhances the conductivity on the surface of the modified GCE. In addition, when the GO/PEDOT:PSS composite was reduced to ErGO/PEDOT:PSS on the surface of the modified electrode, the calculated R_2 was decreased to 104.7 Ω. This indicates an enhanced electronic

https://doi.org/10.1021/acsomega.2c06791
ACS Omega 2023, 8, 3258−3269

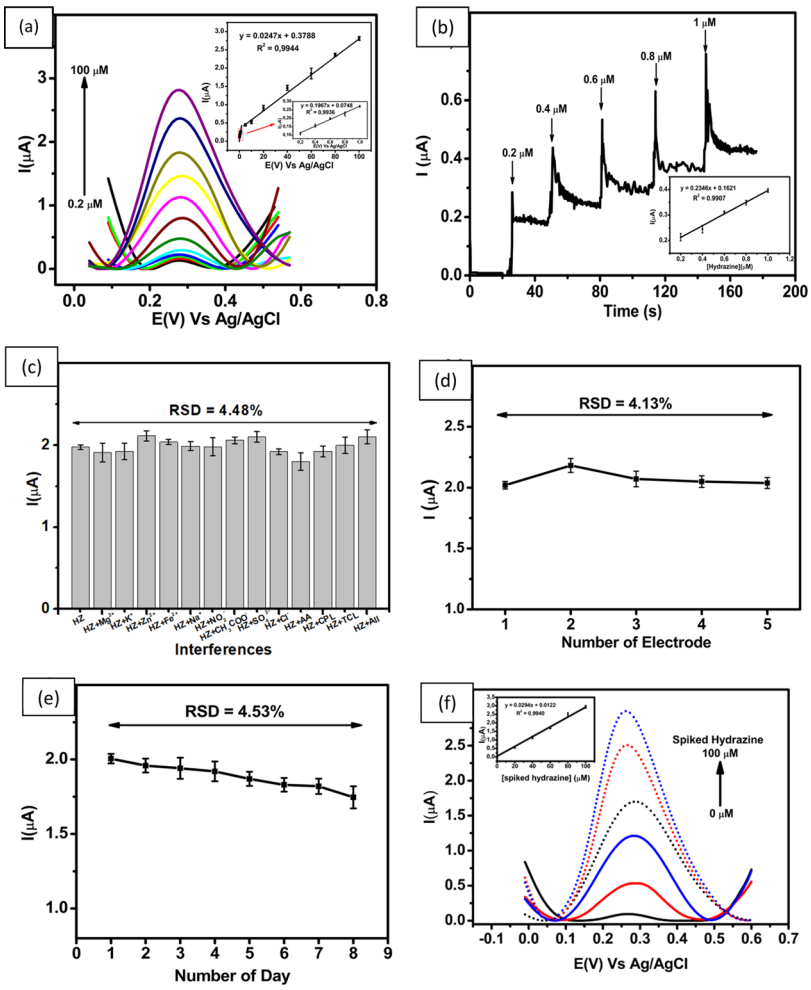

Figure 5. (a) DPV curves obtained from different concentrations of hydrazine (0.2−100 μM), (b) Chronoamperograms in the presence of 0.1 M buffer phosphate at pH 7.0 for the detection of hydrazine at different concentrations. Inset: linear relationship between peak current and the various concentrations of hydrazine, (c) Variation in the response current in the measurement of hydrazine in the presence of several interferences and combined interferences when measured with ErGO/PEDOT:PSS-modified GCE, (d) Reproducibility of the hydrazine measurements at a concentration of 60 μM using five different electrodes, (e) Stability of hydrazine measurements at a concentration of 60 μM over 8 consecutive days, and (f) DPV of hydrazine determination from the river water sample by the standard addition method in the concentration range of 0−100 μM. Inset Figure: linear relationship between the spiked concentration of hydrazine with the peak current.

conductivity for ErGO/PEDOT:PSS compared to GO/PEDOT:PSS, which can be attributed to the following three important points. First, the presence of ErGO in the composite material increases the rate of electron transport and increases the surface area of the modified electrode.[51] Second, PEDOT;PSS, as a p-type conducting polymer, acts as a matrix that donates holes for electro-oxidation.[54,55] Ultimately, third, the electrocatalytic properties of the ErGO/PEDOT:PSS composite are improved as a result of the synergistic interactions between these two materials.[41] Therefore, this composite material possesses the best electrocatalytic and conductivity properties, which indicates intriguing possibilities for further study of its electrochemical performances as a hydrazine sensor.

3.4. Effect of the Scan Rate. To study the scan rate of hydrazine oxidation at the GCE modified with ErGO/PEDOT:PSS, cyclic voltammograms were recorded in the presence of 100 μM hydrazine in 0.1 M phosphate buffer at pH 7 at different scan rates (25, 50, 100, 150, and 200 mV s^{-1}). As shown in Figure 4a the peak current of hydrazine oxidation (I_{pa}) increased with the scan rate from 25 to 200 mV s^{-1}. In addition, the inset image of Figure 4a shows a corresponding calibration plot of I_{pa} vs $\nu^{1/2}$ (I_{pa} = 3.855x + 11.034; R^2 = 0.9922), which exhibits an excellent linear relationship between I_{pa} and $\nu^{1/2}$. This result indicates that the electrochemical reaction of hydrazine on the surface of GCE modified with ErGO/PEDOT:PSS was controlled by the diffusion process. As shown in the inset of Figure 4a, as the scan rate increases, the peak potential is slightly shifted toward positive, which also confirms the irreversible reaction of the hydrazine oxidation.

Evaluation of the effective surface area of three different electrodes was studied by the cyclic voltammetry technique using 1 mM $K_3[Fe(CN)_6]$. A cyclic voltammogram was obtained by measuring 1 mM $K_3[Fe(CN)_6]$ in 0.1 M pH 7 phosphate buffer, using bare GCE, GO/PEDOT:PSS/GCE, and ErGO/PEDOT:PSS/GCE (data not shown). ErGO/PEDOT:PSS/GCE showed the highest oxidation peak (I_{pa} = 16.85 μA) and the highest reduction peak (I_{pc} = 17.20 μA) among these electrodes. In addition, the oxidation and reduction potentials have shifted, which indicated that electron transfer could occur more easily in ErGO/PEDOT:PSS. This

https://doi.org/10.1021/acsomega.2c06791
ACS Omega 2023, 8, 3258−3269

Table 1. Comparison of the Analytical Performance from the Proposed Hydrazine Sensor with Previous Sensors

technique	electrode	linear range (μM)	LOD (μM)	sensitivity (μA mM^{-1})	references
CV	MWCNT[a]@CA$_{DE}$[b]/GCE	0−1000	8.8	21.1	62
LSV	Ag-Ni/rG/GCE	1−1050	0.3	28.4	70
DPV	TiO$_2$/PANI[c]/AuNPs/GCE	0.9−1200	0.1	11.6	71
amperometric	MSRG[d]/Au/GCE	2−30; 30−1500	0.5	32.1; 18.8	72
amperometric	ZIF-8[e]-ErGO/GCE	0.1−260; 260−1160	0.032	145.7; 31.5	73
DPV	Fe-rGO/Mn-Spinel/GCE	0.045−105; 106−653	0.0085	19.3; 20.3	74
LSV	AuNP/MnO$_x$-VO$_x$[f]/ERGO/GCE	30−1000	3.0	150	75
DPV	ErGO/PEDOT:PSS/GCE	0.2−1; 1−100	0.01	196.7; 24.7	this work

[a]Multiwalled carbon nanotubes. [b]CA derived from demethylation of 2-methoxyphenol. [c]Polyaniline. [d]MoS$_2$-reduced graphene. [e]Zeolitic imidazolate framework-8. [f]Multivalent metal oxide.

suggests that the ErGO/PEDOT:PSS modifier shows a synergistic increase in the effective area for the electrode surface and electron transfer.[66] Based on the above results regarding the investigations of measurement of 1.0 mM $K_3[Fe(CN)_6]$ in 0.1 phosphate buffer at pH 7, the effective area for the bare GCE, GO/PEDOT:PSS/GCE, and ErGO/PEDOT:PSS/GCE can be calculated using the Randles−Sevcik equation, eq 4.

$$i_p = (2.687 \times 10^5) n^{3/2} v^{1/2} A D^{1/2} C \quad (4)$$

where i_p is the peak current for hydrazine oxidation (ampere), n is the number of transferred electrons during $K_3[Fe(CN)_6]$ redox reaction (1), D is the coefficient of diffusion (6.70×10^{-6} cm^2 s^{-1} as previously reported[67]), A is the effective area of the electrode (cm^2), ν is the scan rate (V s^{-1}), and C is the concentration of $K_3[Fe(CN)_6]$ solution (mol cm^{-3}). From this equation, the effective area of the electrode (A) for the GCE modified with ErGO/PEDOT:PSS is calculated as 0.076 cm^2, which is higher than those of GO/PEDOT:PSS and bare GCE, evaluated as 0.062 and 0.006 cm^2, respectively. These results showed that the GCE modified with ErGO/PEDOT:PSS was approximately 13 times higher than unmodified GCE. It is obvious that the modification of the GCE surface with the composites ErGO and PEDOT:PSS significantly improved the electroactive surface area of the electrodes. Therefore, GCE modified with ErGO/PEDOT:PSS has the highest catalytic activity for hydrazine oxidation relative to bare GCE.

3.5. Chronoamperometric Studies of the Modified Electrode. The diffusion coefficient of hydrazine can be determined by performing chronoamperometry experiments in a series of concentrations for ErGO/PEDOT:PSS-modified GCE. As shown in the inset in Figure 4b, the chronoamperograms indicate that an increase of the anodic current corresponds to the increasing concentration of hydrazine ranging from 20 to 100 μM. A diffusion coefficient (D) related to the current obtained from the electrochemical reaction of the ErGO/PEDOT:PSS film on GCE can be deduced using the Cottrell equation

$$I = nFACD^{1/2}\pi^{-1/2}t^{-1/2} \quad (5)$$

where n is the total number of electrons involved in the oxidation of hydrazine (4), D is the diffusion coefficient for hydrazine (cm^2 s^{-1}), C is the bulk concentration of hydrazine (mol cm^{-3}), and A is the electrode area (0.07 cm^2). This equation indicates that the plot of I vs $t^{-1/2}$ at different concentrations of hydrazine from 20 to 100 μM was linear. The slopes from the obtained calibration curve were then plotted vs the hydrazine concentration, as shown in Figure 4b, From this, the value of the diffusion coefficient for hydrazine was calculated to be about 8.19×10^{-5} cm^2 s^{-1}, which is comparable to the values reported in previous studies (2.5×10^{-5} cm^2 s^{-1} as reported in ref 68 and 8.3×10^{-5} cm^2 s^{-1}, as described in ref 69).

3.6. Electroanalytical Performance of GCE Modified with ErGO/PEDOT:PSS for the Detection of Hydrazine. *3.6.1. Linearity, Limit of Detection, and Limit of Quantitation.* The electrochemical performance of the GCE modified with ErGO/PEDOT:PSS has been studied for several parameters, including linearity, LOD, and limit of quantitation, using DPV. Figure 5a shows the assessment for the linearity obtained from the DPV (0.2−1; 1−100 μM) in 0.1 M phosphate buffer at pH 7, and a scan rate of 50 mV s^{-1}. The results clearly show that the peak current increases linearly with increasing hydrazine concentration. In addition, the inset of Figure 5a shows the corresponding calibration plot of I_{pa} vs hydrazine with DPV in a concentration range of 0.2−1.0 μM ($I_{pa} = 0.1967x + 0.0748$; $R^2 = 0.9936$) and 1.0−100 μM ($I_{pa} = 0.0247x + 0.3788$; $R^2 = 0.9944$). The investigation of this linearity study shows that the values of the LOD and the LOQ are 0.01 μM (3.20×10^{-4} μg mL^{-1}) and 0.03 μM (9.61×10^{-4} μg mL^{-1}), respectively. The value of the LOD obtained from this work was lower than the allowable threshold limit value (TLV) of 0.312 μM (10 ppb), as suggested by the EPA.[17] Therefore, it can be assumed that this sensor is sensitive to hydrazine detection and potentially could be used in real samples of river water.

Chronoamperometric studies were also used for quantitative analysis of hydrazine with the ErGO/PEDOT:PSS-modified GCE, as shown in Figure 5b. A potential of 0.3 V was selected as the oxidation potential of hydrazine for achieving good sensitivity in measurements. As shown in Figure 5b, the current−time curves illustrated that the responses of ErGO/PEDOT:PSS were modified by successive additions of hydrazine in different concentrations (0.2−1 μM) under stirring in 0.1 M phosphate buffer at pH 7. The oxidation currents of hydrazine increased with each addition to reach a steady state. The oxidation current showed a good linear relationship with the concentrations by the following equation $I_{pa} = 0.6815x + 0.259$; $R^2 = 0.9910$ in a concentration range of 0.2−1.0 μM, as shown in the inset of Figure 5b. This shows the corresponding calibration plot of I_{pa} vs hydrazine by amperometry, which exhibits an excellent linear relationship between I_{pa} and hydrazine concentration.

The analytical performance of ErGO/PEDOT:PSS-modified GCE for hydrazine determination has been compared with a number of previously reported sensors. The analytical parameters given in Table 1 show comparable performance of hydrazine sensors in terms of the linear range, LOD, and

https://doi.org/10.1021/acsomega.2c06791
ACS Omega 2023, 8, 3258−3269

sensitivity from the other sensors. The excellent performance of this proposed hydrazine sensor can be attributed to the presence of the ErGO/PEDOT:PSS composite in the structure of the sensor. This composite offers high conductivity, as well as a high surface area and can therefore accelerate the electron transfer process toward the surface of modified electrodes.

3.6.2. Selectivity of the Sensor. An electrochemical sensor must show noninterfering properties according to some common interfering agents to meet the requirement of a highly effective and selective detection of analytes. Selectivity studies of this proposed hydrazine sensor in relation to the presence of other ions in water were performed using DPV. DPV measurements were performed with 60 μM hydrazine solution in 0.1 M phosphate buffer at pH 7 in the presence of 60 μM various ions (Mg^{2+}, K^+, Zn^{2+}, Fe^{2+}, Na^+, NO_2^-, CH_3COO^-, SO_4^{2-},Cl^-, ascorbic acid, chlorophenol, triclosan, and combined interferences). As shown in Figure 5c, the response current of GCE modified with ErGO/PEDOT:PSS presents no obvious change (with a standard error of less than 7%) when several possible ions were added, which indicates that this proposed sensor can maintain its current response and remain free from the influence of interfering ions. In addition, the value of relative standard deviation (RSD) is in the range of 91−107% (Table 2) and is thus in the acceptable analytical range.[76]

Table 2. Interference Effect and Recovery Value of Hydrazine (HZ) Determination at 60 μM

interferences	interference ratio level (interference:HZ)	I_{HZ} (μA)	recovery (%)
		2.0 ± 0.0	
Mg^{2+}	1:1	1.9 ± 0.2	96.7
K^+	1:1	1.9 ± 0.2	97.4
Zn^{2+}	1:1	2.1 ± 0.1	107.0
Fe^{2+}	1:1	2.0 ± 0.1	103.2
Na+	1:1	2.0 ± 0.1	100.7
NO_2^-	1:1	2.0 ± 0.2	100.3
CH_3COO^-	1:1	2.1 ± 0.1	104.3
SO_4^{2-}	1:1	2.1 ± 0.1	106.5
Cl^-	1:1	1.9 ± 0.2	97.3
ascorbic acid	1:1	1.8 ± 0.1	91.1
chlorophenol	1:1	1.9 ± 0.1	100.8
triclosan	1:1	2.0 ± 0.1	103.9
all	1:1	2.1 ± 0.2	105.3

3.6.3. Reproducibility and Stability. To serve as an effective electrochemical sensor, ErGO/PEDOT:PSS-modified GCE must be evaluated for its reproducibility and stability through DPV analysis. Reproducibility was evaluated using five different electrodes for the measurement of 60 μM hydrazine in 0.1 M pH 7 phosphate buffer as an electrolyte at a scan rate of 50 mV s^{-1}. From this investigation, a value of relative standard deviation (RSD) of 4.13% was obtained using five different electrodes as presented in Figure 5d. Meanwhile, the stability of the electrode was studied by measuring 60 μM hydrazine in 0.1 pH 7 M phosphate buffer using a similar electrode for 8 consecutive days and yielded an RSD value of 4.53%, as shown in Figure 5e. It can be concluded that the proposed hydrazine sensor based on ErGO/PEDOT:PSS-modified GCE provides good reliability in its analytical performances to be employed in real samples such as from river water.

3.7. Detection of Hydrazine in River Water Samples. To further evaluate the applicability of the GCE modified with ErGO/PEDOT:PSS, various samples were prepared by adding a certain concentration of hydrazine (20−100 μM) to river water samples. As shown in Figure 5f, the as-fabricated sensor displays a similar successive rising current response with respect to the increase of the increasingly spiked concentration of hydrazine. The results of hydrazine determination obtained from the electrochemical technique were then compared with the results of the standard method, using spectrophotometric techniques. The value of the hydrazine concentration in river sample samples was obtained in triplicate experiments by both electrochemical and spectrophotometry techniques. As seen in Table 3, the concentration of hydrazine measured with spectrophotometry is slightly higher than the value obtained from electrochemical techniques. This difference might be due to the nonhomogeneity of the assay when the measurement of hydrazine was performed. In addition, the hydrazine concentration obtained from both techniques exceeds the allowable threshold limit value (TLV) suggested by the EPA. Therefore, it can be concluded that the sample taken from river water was contaminated by hydrazine and needs to be treated further.

Table 3. Comparison of Hydrazine Concentrations in River Water Samples Determined with Electrochemical and Spectrophotometric Techniques

method	concentration (μM)	maximum concentration (μM)
electrochemical	1.53 ± 0.12	0.312
spectrophotometry	1.56 ± 0.02	0.312

4. CONCLUSIONS

We successfully demonstrated the employment of a hydrazine sensor based on material composite of ErGO and PEDOT:PSS drop cast onto the GCE surface. Before being used for hydrazine sensors, the composite material ErGO/PEDOT:PSS was characterized by Raman, FTIR, and SEM techniques, as well as EIS studies. The performance of the hydrazine sensor has been successfully quantified in a wide linear range of concentration (0.2−100 μM) and a low LOD of 0.01 μM, which is below the hydrazine TLV established by the EPA (0.312 μM). A low LOD indicates that the hydrazine sensor suggested that the high sensing performance is due to both high electrochemical conductivity and large effective surface area of the ErGO/PEDOT:PSS composite. The proposed hydrazine sensor displayed adequate sensitivity, stability, reproducibility, and selectivity in the selected cations and anions. Comparing the performance of the proposed hydrazine sensor with standard methods (spectrophotometric technique), it was shown that this sensor could be used in the samples of river water. Therefore, the proposed hydrazine sensor demonstrates that the developed method has potential applications for environmental water monitoring.

AUTHOR INFORMATION

Corresponding Author

Wulan Tri Wahyuni − *Department of Chemistry, Faculty of Mathematics and Natural Sciences, IPB University, Bogor, West Java 16680, Indonesia; Tropical Biopharmaca Research Center, Institute of Research and Community Empowerment, IPB University, Bogor, West Java 16680,*

https://doi.org/10.1021/acsomega.2c06791
ACS Omega 2023, 8, 3258−3269

Indonesia; orcid.org/0000-0002-3071-4974;
Email: wulantriws@apps.ipb.ac.id

Authors

Hemas Arif Rahman − *Department of Chemistry, Faculty of Mathematics and Natural Sciences, IPB University, Bogor, West Java 16680, Indonesia*

Mohamad Rafi − *Department of Chemistry, Faculty of Mathematics and Natural Sciences, IPB University, Bogor, West Java 16680, Indonesia; Tropical Biopharmaca Research Center, Institute of Research and Community Empowerment, IPB University, Bogor, West Java 16680, Indonesia*

Budi Riza Putra − *Research Center for Metallurgy, National Research and Innovation Agency (BRIN), South Tangerang, Banten 15314, Indonesia*

Complete contact information is available at:
https://pubs.acs.org/10.1021/acsomega.2c06791

Notes

The authors declare no competing financial interest.

■ ACKNOWLEDGMENTS

The authors thank the Kegiatan Rumah Program Sains Fundamental Molekuler Organisasi Riset Nanoteknologi dan Material Badan Riset dan Inovasi Nasional (BRIN) TA 2022 for its support, with the code number of RP ORNM of 110 and letter number B-1701/III.10/PR.03.08/9/2022.

■ REFERENCES

(1) Huang, S.; Zheng, L.; Zheng, S.; Guo, H.; Yang, F. First Fluorescence Sensor for Hydrazine Ion: An Effective "Turn-On" Detection Based on Thiophene-Cyanodistyrene Schiff-Base. *J. Photochem. Photobiol., A* **2022**, *427*, No. 113851.

(2) Kim, S.-W.; Park, S.-Y.; Roh, C.-H.; Shim, J.-H.; Kim, S-B. Effect of Corrosion Inhibitors on SA106 Grade B Carbon Steel in H_2SO_4-N_2H_4 Solution for the Hydrazine-Based Reductive Metal Ion Decontamination Process. *Chem. Pap.* **2022**, *76*, 6517−6522.

(3) Riggs, A. S.; Borth, D. M.; Tutty, D. G.; Yu, W. S.; et al. Determination of Hydrazine in Maleic Hydrazide Technical and Pesticide Formulations by Gas Chromatography: Collaborative Study. *J. AOAC Int.* **2008**, *91*, 5−12.

(4) Chen, Y.; Mo, W.; Cheng, Z.; Kong, F.; Chen, C.; Li, X.; Ma, H. A Portable System Based on Turn-On Fluorescent Probe for the Detection of Hydrazine in Real Environment. *Dyes Pigm.* **2022**, *198*, No. 110004.

(5) Yu, Y.; Lee, S. J.; Theerthagiri, J.; Lee, Y.; Choi, M. Y. Architecting the AuPt Alloys for Hydrazine Oxidation as an Anolyte in Fuel Cell: Comparative Analysis of Hydrazine Splitting and Water Splitting for Energy-Saving H_2 Generation. *Appl. Catal., B* **2022**, *316*, No. 121603.

(6) Li, M.; Zhou, Z.; Hu, L.; Wang, S.; Zhou, Y.; Zhu, R.; Chu, X.; Vinu, A.; Wan, T.; Cazorla, C.; Yi, J.; Chu, D. Hydrazine Hydrate Intercalated 1T-Dominant MoS_2 with Superior Ambient Stability for Highly Efficient Electrocatalytic Applications. *ACS Appl. Mater. Interfaces* **2022**, *14*, 16338−16347.

(7) Wang, Z.; Zhang, Y.; Meng, Z.; Li, M.; Zhang, C.; Yang, L.; Yang, Y.; Xu, X.; Wang, S. Development of a Ratiometric Fluorescent Probe with large Stokes Shift and Emission Wavelength Shift for Real-Time Tracking of Hydrazine and its Multiple Applications in Environmental Analysis and Biological Imaging. *J. Hazard. Mater.* **2022**, *422*, No. 126891.

(8) Tajik, S.; Askari, M. B.; Ahmadi, S. A.; Nejad, F. G.; Dourandish, Z.; Razavi, R.; Beitollahi, H.; Di Bartolomeo, A. D. Electrochemical Sensor Based on $ZnFe_2O_4$/RGO Nanocomposite for Ultrasensitive Detection of Hydrazine in Real Samples. *Nanomaterials* **2022**, *12*, 1−10.

(9) Lu, Z.; Fan, W.; Shi, X.; Lu, Y.; Fan, C. Two Distinctly Separated Colorimetric NIR Fluorescent Probe for Fast Hydrazine Detection in Living Cells and Mice upon Independent Excitations. *Anal. Chem.* **2017**, *89*, 9918−9925.

(10) Liu, Z.; Yang, Z.; Chen, S.; Liu, Y.; Sheng, L.; Tian, Z.; Huang, D.; Xu, H. Smart A Reaction-Based Fluorescence Probe for Ratio Detection of Hydrazine and Its Application in Living Cells. *Microchem. J.* **2020**, *156*, No. 104809.

(11) Lv, H.; Sun, H.; Wang, S.; Kong, F. A Novel Dicyanoisophorone Based Red-Emitting Fluorescent Probe with a Large Stokes Shift for Detection of Hydrazine in Solution and Living Cells. *Spectrochim. Acta, Part A* **2018**, *196*, 160−167.

(12) Preethi, S.; Sangaranarayanan, M. V. Shape-Controled Electrodeposition of Silver Using Chitosan as Structure-Directing Agent on Disposable Pencil Graphite Electrodes: Low-Cost Electrocatalysts for the Detection of Hydrogen Peroxide and Hydrazine Hydrate. *J. Solid State Electrochem.* **2020**, *24*, 2773−2788.

(13) Teoman, I.; Karakaya, S.; Dilgin, Y. Sensitive and Rapid Flow Injection Amperometric Hydrazine Sensor Using an Electrodeposited Gold Nanoparticle Graphite Pencil Electrode. *Anal. Lett.* **2019**, *52*, 2041−2056.

(14) Ayaz, S.; Dilgin, Y. Flow Injection Amperometric Determination of Hydrazine Based on Its Electrocatalytic Oxidation at Pyrocatechol Violet Modified Pencil Graphite Electrode. *Electrochim. Acta* **2017**, *258*, 1086−1095.

(15) Tang, Y.-Y.; Kao, C.-L.; Chen, P.-Y. Electrochemical Detection of Hydrazine Using a Highly Sensitive Nanoporous Gold Electrode. *Anal. Chim. Acta* **2012**, *711*, 32−39.

(16) Su, H.; Wang, J.; Yue, X.; Wang, B.; Song, X. A Ratiometric Fluorescent Probe with Large Stokes Shift and Emission Shift for Sensing Hydrazine in Living Organisms. *Spectrochim. Acta, Part A* **2022**, *274*, No. 121096.

(17) Crapnell, R. D.; Banks, C. E. Electroanalytical Overview: The Electroanalytical Sensing of Hydrazine. *Sens. Diagn.* **2022**, *1*, 71−86.

(18) Verma, K. K.; Srivastava, A.; Ahmed, J.; Bose, S. Titrimetric Determination of Some Organic Compounds with Bromine Chloride. *Talanta* **1978**, *25*, 469−475.

(19) Lim, H.-H.; Choi, K.-Y.; Shin, H.-S. In-Solution Derivatization and Headspace Gas Chromatography-Mass Spectrometry for 56 Carbonyl Compounds in Tobacco Heating Products, Traditional Tobacco Products and Flavoring Capsules. *Chromatographia* **2022**, *85*, 699−717.

(20) Song, L.; Gao, D.; Li, S.; Wang, Y.; Liu, H.; Jiang, Y. Simultaneous Quantitation of Hydrazine and Acetylhydrazine in Human Plasma by High Performance Liquid Chromatography-Tandem Mass Spectrometry After Derivatization with p-tolualdehyde. *J. Chromatogr. B* **2017**, *1063*, 189−195.

(21) Yan, L.; Zhang, S.; Xie, Y.; Mu, X.; Zhu, J. Recent Progress in Development of Fluorescent Probes for the Detection of Hydrazine (N_2H_4). *Crit. Rev. Anal. Chem.* **2022**, *52*, 210−229.

(22) Liu, J.; Jiang, J.; Dou, Y.; Zhang, F.; Liu, X.; Qu, J.; Zhu, Q. A Novel Chemiluminescent Probe for Hydrazine Detection in Water and HeLa Cells. *Org. Biomol. Chem.* **2019**, *17*, 6975−6979.

(23) Xu, G.; Guo, N.; Zhang, Q.; Wang, T.; Song, P.; Xia, L. An Ultrasensitive Surface-Enhanced Raman Scattering Sensor for the Detection of Hydrazine via the Schiff Base Reaction. *J. Hazard. Mater.* **2021**, *424*, No. 127303.

(24) Kaur, A.; Chakraborty, U.; Chauhan, M.; Sharma, R.; Kaur, G.; Chaudhary, G. R. Choline Acetate Modified ZnO Nanostructure as Efficient Electrochemical Sensor for Hydrazine Detection. *Electrochim. Acta* **2022**, *419*, No. 140384.

(25) Hira, S. A.; Annas, D.; Nagappan, S.; Kumar, Y. A.; Song, S.; Kim, H.-J.; Park, S.; Park, K. H. Electrochemical Sensor Based on Nitrogen-Enriched Metal-Organic Framework for Selective and Sensitive Detection of Hydrazine and Hydrogen Peroxide. *J. Environ. Chem. Eng.* **2021**, *9*, No. 105182.

(26) Liang, C.; Ling, H.; Guo, W.; Lu, X.; Yu, D.; Fan, S.; Zhang, F.; Qu, F. Amperometric Sensor Based on ZIF/g-C_3N_4/RGO Heterojunction Nanocomposite for Hydrazine Detection. *Microchim. Acta* **2021**, *188*, No. 48.
(27) Wang, H.-B.; Zhang, H.-D.; Xu, L.-L.; Gan, T.; Huang, K.-J.; Liu, Y.-M. Electrochemical Biosensor for Simultaneous Determination of Guanine and Adenine Based on Dopamine-Melanin Colloidal Nanospheres-Graphene Composites. *J. Solid State Electrochem.* **2014**, *18*, 2435−2442.
(28) Wang, H.-B.; Zhang, H.-D.; Zhang, Y.-H.; Chen, H.; Xu, L.-L.; Huang, K.-J.; Liu, Y.-M. Tungsten disulfide nano-flowers/silver nanoparticles composites based electrochemical sensor for theophylline determination. *J. Electrochem. Soc.* **2015**, *162*, B173.
(29) Liu, Z.; Tao, J.; Zhu, Z.; Zhang, Y.; Wang, H.; Pang, P.; Wang, H.; Yang, W. A Sensitive Electrochemical Assay for T4 Polynucleotide Kinase Activity Based on Fe_3O_4@TiO_2 and Gold Nanoparticles Hybrid Probe Modified Magnetic Electrode. *J. Electrochem. Soc.* **2022**, *169*, No. 027504.
(30) Rana, D. S.; Thakur, N.; Thakur, S.; Singh, D. Electrochemical Determination of Hydrazine by Using MoS_2 Nanostructure Modified Gold Electrode. *Nanofabrication* **2022**, *7*, No. e002.
(31) Singh, P.; Singh, K. R. B.; Verma, R.; Prasad, P.; Verma, R.; Das, S. N.; Singh, J.; Singh, R. P. Preparation, Antibacterial Activity, and Electrocatalytic Detection of Hydrazine Based on Biogenic $CuFeO_2$/PANI Nanocomposites Synthesized Using *Aloe barbadensis* Miller. *New J. Chem.* **2022**, *46*, 8805−8816.
(32) Yang, J.; Yang, L.; Tang, X.; Zhang, Y.; Dong, Q.; He, Z.; Li, N.; Huang, K.; Luo, H.; Xiong, X. ZIF Derived N-CoS_2@graphene Rhombic Dodecahedral Nanocomposites: As a High Sensitivity Sensor for Hydrazine. *Sens. Actuators, B* **2022**, *351*, No. 130967.
(33) Chiani, E.; Azizi, S. N.; Ghasemi, S. Superior Electrocatalyst Based on Mesoporous Silica Nanoparticles/Carbon Nanotubes Modified by Platinum-Copper Bimetallic Nanoparticles for Amperometric Detection of Hydrazine. *Int. J. Hydrogen Energy* **2022**, *47*, 20087−20102.
(34) Soundiraraju, B.; Anthony, A. M.; Pandurangan, P.; George, B. K. Electrochemical Behavior of Chromium Carbide MXene Modified Electrodes: Hydrazine Sensing. *Mater. Today Commun.* **2022**, *32*, No. 103982.
(35) Xing, Y.; Tang, X.; Ling, C.; Zhang, Y.; He, Z.; Ran, G.; Yu, H.; Huang, K.; Zou, Z.; Xiong, X. Three-Dimensional Setaria viridis-like $NiCoSe_2$ Nanoneedles Array: As an Efficient Electrochemical Hydrazine Sensor. *Colloids Surf., A* **2022**, *650*, No. 129549.
(36) Wang, W.; Zhao, Z.; Lei, Q.; Xu, H.; Hu, J.; Chen, L. Hierarchical Layered Double NiCo Oxide/Core-Shell Arrays Structure Functionalization with Au Nanoparticles for Highly Sensitive Hydrazine Determination. *Microchem. J.* **2022**, *181*, No. 107826.
(37) Xu, J.; Long, X.; Zhang, J.; Wu, S. Highly Sensitive Electrochemical Sensor Based on Novel Ag Nps/PPTI Films for Detection of Hydrazine. *Pigm. Resin Technol.* **2022**, No. 120.
(38) Ahmad, K.; Kim, H. Synthesis of MoS_2/WO_3 Hybrid Composite for Hydrazine Sensing Applications. *Mater. Sci. Semicond. Process.* **2022**, *148*, No. 106803.
(39) Khan, M. E.; Mohammad, A.; Ali, W.; Khan, A. U.; Hazmi, W.; Zakri, W.; Yoon, T. Excellent Visible-Light Photocatalytic Activity Towards the Degradation of Tertracycline Antibiotic and Electrochemical Sensing of Hydrazine by SnO_2-CdS Nanostructures. *J. Cleaner Prod.* **2022**, *349*, No. 131249.
(40) Ma, X.; Lu, K.; Yuan, B.; Shi, W.; Yu, L.; Zhao, W. Anion Engineering Guided MOF-to-Hollow Nickel Phosphate Transformation Enabling Robust Electrochemical Platforms for Detection of Hydrogen Peroxide and Hydrazine. *Sens. Actuators, B* **2022**, *369*, No. 132373.
(41) Putra, B. R.; Nisa, U.; Heryanto, R.; Rohaeti, E.; Khalil, M.; Izzataddini, A.; Wahyuni, W. T. Facile A Electrochemical Sensor Based on a Composite of Electrochemically Reduced Graphene Oxide and a PEDOT:PSS Modified Glassy Carbon Electrode for Uric Acid Detection. *Anal. Sci.* **2022**, *38*, 157−166.
(42) Wang, Q.; Zhang, J.; Xu, Y.; Wang, Y.; Wu, L.; Weng, X.; You, C.; Feng, J. A One-Step Electrochemically Reduced Graphene Oxide Based Sensor for Sensitive Voltammetric Determination of Furfural in Milk Products. *Anal. Methods* **2021**, *13*, 56−63.
(43) Gevaerd, A.; Watanabe, E. Y.; Fernandes, K.; Papi, M. A. P.; Banks, C. E.; Bergamini, M. F.; Marcolino-Junior, L. H. Electrochemically Reduced Graphene-Oxide as Screen-Printed Electrode Modifier for Fenamiphos Determination. *Electroanalysis* **2020**, *32*, 1689−1695.
(44) Báez, D. F.; Tapia, F.; Sieraa-Rosales, P.; Bollo, S. *In Situ* Electroreduction of Graphene Oxide: Increased Sensitivity for the Determination of NADH. *Electroanalysis* **2019**, *31*, 461−467.
(45) Nemakal, M.; Aralekallu Mohammed, I.; Mohammed, I.; Swamy, S.; Swamy, S.; Sannegowda, L. K. Electropolymerized octabenzimidazole phthalocyanine as an amperometric sensor for hydrazine. *J. Electroanal. Chem.* **2019**, *839*, 238−246.
(46) Dada, O. J.; Villaroman, D. Superior Electronic and Dielectric Properties of Corrugated Electrochemically Reduced Graphene over Graphene Oxide Papers. *J. Electrochem. Soc.* **2019**, *166*, D21−D36.
(47) Gao, W.; Debiemme-Chouvy, C.; Lahcini, M.; Perro, H.; Sel, O. Tuning Charge Storage Properties of Supercapacitive Electrodes Evidenced by In Situ Gravimetric and Viscoelastic Explorations. *Anal. Chem.* **2019**, *91*, 2885−2893.
(48) Jing, M.; Zhang, C.; Chi, X.; Yang, Y.; Liu, J.; Fan, X.; Yan, C.; Fang, D. Gradient-Microstructural Porous Graphene Gelatum/Flexible Graphite Plate Integrated Electrode for Vanadium Redox Flow Batteries. *Int. J. Hydrogen Energy* **2020**, *45*, 916−923.
(49) Yasmin, S.; Cho, S.; Jeon, S. Electrochemically Reduced Graphene-Oxide Supported Bimetallic Nanoparticles Highly Efficient for Oxygen Reduction Reaction with Excellent Methanol Tolerance. *Appl. Surf. Sci.* **2018**, *434*, 905−912.
(50) Joo, Y.; Ahmed, M. S.; Han, H. S.; Jeon, S. Preparation of Electrochemically Reduced Graphene Oxide-Based Silver-Cobalt Alloy Nanocatalysts for Efficient Oxygen Reduction Reaction. *Int. J. Hydrogen Energy* **2017**, *42*, 21751−21761.
(51) Urhan, B. K.; Doğan, H. Ő.; Ĉepni, E.; Eryigit, M.; Demir, Ű.; Ni Ozer, T. Ő. Ni(OH)$_2$-electrochemically Reduced Graphene Oxide Nanocomposites as Anode Electrocatalyst for Direct Ethanol Fuel Cell in Alkaline Media. *Chem. Phys. Lett.* **2021**, *763*, No. 138208.
(52) Zhuo, H.-Y.; Zhang, X.; Liang, J.-X.; Yu, Q.; Xiao, H.; Li, J. Theoretical Understandings of Graphene-Based Metal Single-Atom Catalysts: Stability and Catalytic Performance. *Chem. Rev.* **2020**, *120*, 12315−12341.
(53) Akaishi, A.; Ushirozako, M.; Matsuyama, H.; Nakamura, J. Structural Stability and Aromaticity of Pristine and Doped Graphene Nanoflakes. *Jpn. J. Appl. Phys.* **2018**, *57*, No. 0102BA.
(54) Nguyen, D. C. T.; Mai, V.-D.; Tran, V.-H.; Vu, V.-P.; Lee, S.-H. Use of Modified PEDOT:PSS/Graphene Oxide Dispersions as a Hole Transport Layer for Inverted Bulk-Heterojunction Organic Solar Cells. *Org. Electron.* **2022**, *100*, No. 106388.
(55) Lera, I. L.; Khasnabis, S.; Wangatia, L. M.; Femi, O. E.; Ramamurthy, P. C. Insights into Electrochemical Behavior and Kinetics of NiP on PEDOT:PSS/Reduced Graphene Oxide as High Performance Electrodes for Alkaline Urea Oxidation. *J. Solid State Electrochem.* **2022**, *26*, 195−209.
(56) Putra, B. R.; Nisa, U.; Heryanto, R.; Khalil, M.; Khoerunnisa, F.; Ridhova, A.; Thaha, Y. N.; Marken, F.; Wahyuni, W. T. Selective Non-Enzymatic Uric Acid Sensing in the Presence of Dopamine: Electropolymerized Poly-Pyrrole Modified with a Reduced Graphene Oxide/PEDOT:PSS Composite. *Analyst* **2022**, *147*, 5334−5346.
(57) Molina, B. G.; Cuesta, S.; Besharatloo, H.; Roa, J. J.; Armelin, E.; Alemán, C. Free-standing Faradaic Motors Based on Biocompatible Nanoperforated Poly(Lactic Acid) Layers and Electropolymerized Poly(3,4-Ethylenedioxythiophene). *ACS Appl. Mater. Interfaces* **2019**, *11*, 29427−29435.
(58) Agarwal, V.; Zetterlund, P. B. Strategies for Reduction of Graphene Oxide-A Comprehensive Review. *Chem. Eng. J.* **2021**, *405*, No. 127018.

https://doi.org/10.1021/acsomega.2c06791
ACS Omega 2023, 8, 3258−3269

(59) Abd-Wahab, F.; Guthoos, H. F. A.; Salim, W. W. A. W. Solid-State rGO-PEDOT:PSS Transducing Material for Cost-Effective Enzymatic Sensing. *Biosensors* **2019**, *9*, 36.
(60) Yan, W.; Li, J.; Zhang, G.; Wang, L.; Ho, D. A Synergistic Self-Assembled 3D PEDOT:PSS/Graphene Composite Sponge for Strectchable Microsupercapacitors. *J. Mater. Chem. A* **2020**, *8*, 554−564.
(61) Aliyev, E.; Filiz, V.; Khan, M. M.; Lee, Y. J.; Abetz, C.; Abetz, V. Structural Characterization of Graphene Oxide: Surface Functional Groups and Fractionated Oxidative Debris. *Nanomaterials* **2019**, *9*, 1180.
(62) Xu, Z.; Songa, J.; Liu, B.; Lv, S.; Gao, F.; Luo, X.; Wang, P. A Conducting Polymer PEDOT:PSS Hydrogel Based Wearable Sensor for Accurate Uric Acid Detection in Human Sweat. *Sens. Actuators, B* **2021**, *348*, No. 130674.
(63) Miao, R.; Compton, R. G. Mechanism of Hydrazine Oxidation at Palladium Electrodes: Long-Lived Radical di-Cation Formation. *Electrochim. Acta* **2021**, *388*, No. 138655.
(64) Kim, G. H.; Hwang, D. H.; Woo, S. I. Thermoelectric Properties of Nanocomposite Thin Films Prepared with Poly(3,4-Ethylenedioxythiophene) Poly(Styrenesulfonate) and Graphene. *Phys. Chem. Chem. Phys.* **2012**, *14*, 3530−3536.
(65) Park, H.; Lee, S. H.; Kim, F. S.; Choi, H. H.; Cheong, I. W.; Kim, J. H. Enhanced Thermoelectric Properties of PEDOT:PSS Nanofilms by a Chemical Dedoping Process. *J. Mater. Chem. A* **2014**, *2*, 6532−6539.
(66) Gharani, M.; Bahari, A.; Ghasemi, S. Preparation of MoS_2-Reduced Graphene Oxide/Au Naohybrid for Electrochemical Sensing of Hydrazine. *J. Mater. Sci.: Mater. Electron.* **2021**, *32*, 7765−7777.
(67) Feng, J.; Lang, G.; Li, T.; Zhang, J.; Zhao, J.; Li, W.; Yang, W.; Jiang, Z. Enhanced Electrochemical Detection Performance of C-Cr2O3 toward Glucose and Hydrazine by Assembling Ni-MPN Coating. *Appl. Surf. Sci.* **2022**, *604*, No. 154548.
(68) Beitollahi, H.; Tajik, S.; Maleh, H. K.; Hosseinzadeh, R. Application of a 1-benzyl-4-ferrocenyl-1H-[1,2,3]-Triazole/Carbon Nanotube Modified Glassy Carbon Electrode for Voltammetric Determination of Hydrazine in Water Samples. *Appl. Organomet. Chem.* **2013**, *27*, 444−450.
(69) Soltaninejad, V. S.; Maleki, A.; Beitollahi, H.; Zare-Dorabei, R. Fabrication of a Sensitive Electrochemical Sensor Based on Modified Screen Printed Electrode for Hydrazine Analysis in Water Samples. *Int. J. Environ. Anal. Chem.* **2020**, 1−18.
(70) Gandhi, M.; Rajagopal, D.; Senthil Kumar, A. S. Facile Electrochemical Demethylation of 2-Methoxyphenol to Surface-Confined Catechol on the MWCNT and Its Efficient Electrocatalytic Hydrazine Oxidation and Sensing Applications. *ACS Omega* **2020**, *5*, 16208−16219.
(71) Meng, Z.; Liu, B.; Li, B. A Sensitive Hydrazine Electrochemical Sensor Based on Ag-Ni Alloy/Reduced Graphene Oxide Composite. *Int. J. Electrochem. Sci.* **2017**, *12*, 10269−10278.
(72) Saeb, E.; Asadpour-Zeynali, K. Facile Synthesis of TiO_2@PANI@Au Nanocomposite as an Electrochemical Sensor for Determination of Hydrazine. *Microchem. J.* **2021**, *160*, No. 105603.
(73) Xie, J.; Yang, H.; Wang, X.; Gao, F. ZIF-8/Electro-reduced Graphene Oxide Nanocomposite for Highly Electrocatalytic Oxidation of Hydrazine in Industrial Wastewater. *Microchem. J.* **2021**, *168*, No. 106521.
(74) Singh, M.; Bhardiya, S. R.; Asati, A.; Sheshma, H.; Rai, A.; Rai, V. K. Design of a Sensitive Electrochemical Sensor Based on Ferrocene-Reduced Graphene Oxide/Mn-Spinel for Hydrazine Detection. *Electroanalysis* **2021**, *33*, 464−472.
(75) Aslışen, B.; Koçak, S. Preparation of Mixed-Valent Manganese-Vanadium Oxide and Au Nanoparticle Modified Graphene Oxide Nanosheets Electrodes for the Simultaneous Determination of Hydrazine and Nitrite. *J. Electroanal. Chem.* **2022**, *904*, No. 115875.
(76) Haque, A.-M. J.; Kumar, S.; Sabate Del Río, J. S.; Cho, Y.-K. Highly Sensitive Detection of Hydrazine by a Disposable, Poly-(Tannic Acid)-Coated Carbon Electrode. *Biosens. Bioelectron.* **2020**, *150*, No. 111927.

https://doi.org/10.1021/acsomega.2c06791
ACS Omega 2023, 8, 3258−3269